AIAA-2000-1623

AEROELASTIC ANALYSIS OF A COMPOSITE WINGBOX WITH VARYING ROOT FLEXIBILITY

Peter W.G. De Baets[*], *Rupinder S. Battoo*[†], *and Dimitri N. Mavris*[‡]

The research looked into the aeroelastic properties and modal response of a composite rectangular wingbox. This research attempted to assess the sensitivity of the flutter speed, divergence speed and modal response when varying the composite skin lay-up, fibre orientation, and the root flexibility of the model. All this research was conducted using the finite element code ASTROS. An attempt was made to cover as extensive a field as possible and identify interesting areas that required further examination. Interesting relations were found between the following properties: *EI*/*GJ* versus fibre orientation and various mode ratios versus root stiffness. These could be linked with the changes in flutter and divergence speed of the composite model. In certain regions of the root flexibility, the flutter and divergence speeds showed dips and peaks. These coincided with changes in modal behaviour and were verified with a visualisation tool.

Objectives of Research

The purpose of this piece of work was to establish the aeroelastic effects of variation of composite fibre orientation, root flexibility, and stacking of plies for a rectangular closed thin-walled wing box. Although many of these features had already been analysed, usually they were treated individually and not considered collectively. A sensitivity analysis was conducted for the root stiffness, fibre orientation and stacking sequence so that their effect on the modal behaviour, flutter and divergence speeds could be analysed; for different laminates. The finite element code used was ASTROS version 11 (*Ref. 8, 9,* and *11*).

The ply-stacking and fibre orientation had been studied systematically in the past (*Ref. 2*, *5, 7,* and *14*). The objective of this research not only entailed these two characteristics but also included root flexibility to determine the effect on the response of a composite wingbox. The approach to this problem required that the three variables would be changed in an organised manner so that conclusions could be made that related to a change in physical property; being ply stacking sequence, fibre orientation, and root stiffness.

The first two variables, fibre orientation and ply stacking sequence, had been modelled with finite elements. The last one however, the root flexibility, was not usually modelled. Therefore an innovative way was found to quickly and efficiently model that feature. The boundary condition was eventually modelled with only two springs. More information is to follow further in the paper.

The investigated aeroelastic properties were flutter and divergence speed. However a possibly even more important characteristic of a wing is its modal behaviour. Therefore, eigenvalues were computed and analysed too. These three plots were then compared with the change in physical properties, which for composites were essentially the effective bending stiffness parameter, *EI*, effective torsional stiffness parameter, *GJ*, and bend-twist structural coupling, *K*.

Finite Element Model

Fibre Reinforced Plastic – Equations

The equations for calculation of the stiffness and bend-twist structural coupling of the composite wingbox – *EI*, *GJ* and *K* – were derived from Chandra *et al.* (*Ref. 3*). These equations are to be read in conjunction with *Figure 1* and were also used in previous research (*Ref. 1*).

[*] Graduate Researcher, Georgia Institute of Technology, Student Member
[†] Managing Director, Baron Consulting Limited , Member
[‡] Asst. Professor, Director ASDL, Georgia Institute of Technology, Member

$$EI = \sum_{k=1}^{N} \iint_{1,2} \overline{C}_{11}^{(k)} \xi^2 \, d\eta \, d\xi + \sum_{l=1}^{M} \iint_{3,4} \overline{C}_{11}^{(l)} \xi^2 \, d\eta \, d\xi$$

$$GJ = \sum_{k=1}^{N} \iint_{1,2} \overline{C}_{66}^{(k)} \hat{\xi}^2 \, d\eta \, d\xi + \sum_{l=1}^{M} \iint_{3,4} \overline{C}_{66}^{(l)} \hat{\eta}^2 \, d\eta \, d\xi$$

$$K = \sum_{k=1}^{N} \iint_{1,2} \overline{C}_{16}^{(k)} \hat{\xi}\xi \, d\eta \, d\xi$$

With:

$$\overline{C}_{11} = \overline{Q}_{11} - \frac{\overline{Q}_{12}^2}{\overline{Q}_{22}}$$

$$\overline{C}_{16} = \overline{Q}_{16} - \overline{Q}_{12}\left(\frac{\overline{Q}_{26}}{\overline{Q}_{22}}\right)$$

$$\overline{C}_{66} = \overline{Q}_{66} - \frac{\overline{Q}_{26}^2}{\overline{Q}_{22}}$$

And:

1,2,3,4, refer to top & bottom skin and front & rear spar respectively

k, refers to a ply on the top or bottom skin

N, total number of plies on the top (1) or bottom (2) skin

l, refers to a ply on the front or rear spar

M, total number of plies on the front (3) or rear (4) spar

c, chord [m]

d, depth [m]

$\overline{Q}$, the stiffness matrix for the k[th] ply in the y-η or y-ξ plane [N/mm^2]

Also :

$$\Lambda = \beta\xi\eta$$

$$\beta = \frac{(c-d)}{(c+d)}$$

$$\hat{\xi} = \frac{d}{d\eta}(\xi + \Lambda)$$

$$\hat{\eta} = \frac{d}{d\xi}(\eta - \Lambda)$$

With:

Λ, the assumed warping function

η, ξ, co-ordinates in the plane of cross-section

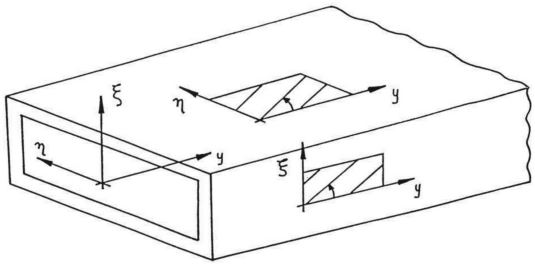

Figure 1 Co-ordinate System Orientations

Model Description

A simple wing box was employed instead of a beam or plate to give greater semblance to a real wing structure. The purpose of retaining a simplified structure was to yield workable results without the added complication of a complex finite-element model. During the project, circumferentially uniform (CUS) and asymmetric (CAS) stiffness models were considered (*Ref. 1*). The composite used during the project was carbon fibre and epoxy resin with the properties in *Table 1*. Further characteristics of the model were summarised in *Table 2* and *Table 3*.

E_{11}	N/m^2	130000 10^6
E_{22}	N/m^2	8900 10^6
G_{12}	N/m^2	4800 10^6
ν_{12}	-	0.28
Density ρ	kg/m^3	1610
Ply Thickness *t*	m	0.17 10^{-3}

Table 1 Composite Properties

	Dimensions
	[m]
Chord	0.100
Depth	0.025
Span	1.000

Table 2 ASTROS Model Dimensions

	Structural Mesh	Aerodynamic Mesh
	[No. of Elements]	[No. of Elements]
Chord	10	5
Depth	2	-
Span	20	25

Table 3 ASTROS Mesh Properties

Root flexibility

The root stiffness was modelled using an RBE2-element and springs. The grid points at the root of the wingbox were all attached to one grid point located at the centre of the wing box root using the RBE2 (*Figure 2*). The RBE2 made the displacements of all

the root grids dependent on the displacements of the centre grid. The connections between the centre grid and wing root are rigid.

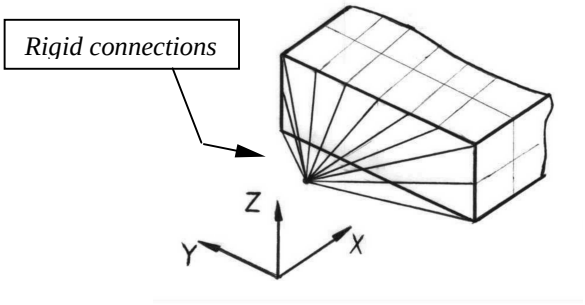

Figure 2 Root Flexibility Modelling

The centre grid was attached to springs whose rotation and translation stiffness properties could be varied. One end of the springs was attached to the grid point with the independent degrees of freedom. The springs simulated rotational and translation stiffness. The other end of the springs was connected to a grounded point. The additional structure, which the RBE-element and springs actually were, did not interfere with the results. This was checked by making the springs very stiff and comparing the result to the clamped case. It appeared that the properties closed-in on the clamped-case values asymptotically.

Laminates Considered

Only symmetric laminates were considered throughout the research in order to contain the scope of the work to a reasonable magnitude. However as mentioned earlier, balanced and unbalanced models were considered. This allowed calculating various *EI* and *GJ* values for the models and the examination of the effect of these variations on the aeroelastic response. The actual laminates considered were chosen in a way such that the *EI*, *GJ* and *K* values were substantially different from each other.

Laminate for the spars was $(+45/-45)_S$ and did not change throughout the research. The first skin laminate had the following ply stacking sequence: $(0/0/\theta/\theta)_S$, and *EI*/*GJ* properties can be found in *Figure 3*. The second skin laminate consisted of the $(0/\theta/\theta/\theta)_S$ ply stacking sequence, and its *EI*/*GJ* properties can be found in *Figure 4*. The cases were presented by fibre orientation and stiffness model. Furthermore, the root stiffness notation 10^{10} meant that the torsion and heaving spring had a stiffness of respectively 10^{10} N/rad and 10^{10} N/mm.

Analysis of Results

The two models, one with the bending and heaving degree of freedom and the other one with the torsion and heaving degree of freedom were discussed respectively. Within that model with the specified boundary condition, subsequent distinction was made between a model with the first laminate and a model with the second laminate. For each different model, conclusions on the flutter, divergence and modal properties were noted.

The graphs with different fibre orientations used the same symbol for opposite fibre angles (i.e. +30 and –30 use the same symbol) however, the positive angles were plotted by a full line whereas the negative fibre angles were plotted by a dashed line. Also note the acronyms used in the graphs for the eigenvalues: ‘OB’ stoods for first out-of-plane bending mode, ‘2OB’ stands for second out-of-plane bending mode, ‘3OB’ stands for third out-of-plane bending mode, ‘IB’ stands for in-plane bending mode and, ‘T’ stands for torsion mode.

First Boundary Condition: Bending and Heaving Degree of Freedom

The boundary condition springs had an out-of-plane bending and heaving degree of freedom. The two laminates considered were the ones previously discussed.

Model with First Laminate

- The evolution of the ratio of the two boundary condition degrees-of-freedom (*Figure 6*) showed a very similar trend like the divergence speeds (*Figure 7*). From 10^3 onwards, the ratio was no longer constant and started an increase to a peak at 10^5. Afterwards the ratio went back down and levelled off at a constant value for the higher root stiffness. It was noted that as soon as the ratio starts increasing, the divergence (and flutter speed too, found in *Figure 5*) dipped and then rose further asymptotically to their clamped case value. Once the peak in the *ratio* was reached, the divergence speeds levelled off at a constant speed. Similar behaviour was noted for CUS models.
- The same ratio (*Figure 7*) had a peak for the 0-degree ply direction and decreased for positive and negative ply angles and the opposite was valid for the divergence speed. The change in divergence speed could thus be related with the *EI*/*GJ* ratio. This effect was also cross-checked with Shirk *et al.* (*Ref. 12*).

- The variation of the out-of-plane bending over second out-of-plane bending ratio (*Figure 7*) and out-of-plane bending over torsion ratio (*Figure 8*) both showed similarities with the change in *EI*/*GJ* ratio. That change in *EI*/*GJ* ratio was mostly due to the peak in the *EI*-value, the bending stiffness parameter.
- The differences between CAS and CUS for flutter and divergence looked significant; however, the non-dimensional speeds showed that in terms of behaviour, there was not that much difference. The only change was the accentuation and more pronounced presence of the peaks and dips for the CUS model.

Visualisation gave insights summed up below. It also proved to be the solution to a certain number of problems. The modes in these figures were labelled according to their final mode shape. The following conclusions refer to *Figure 9*.

- The two first modes started out as almost two rigid body movements, which were the two degrees of freedom of the boundary conditions. These did not show much change until the root stiffness reached 10^3. At this point, they were still distinguishable as rigid body movement (RBM). At 10^4, the picture had changed significantly: the first mode was the first out-of-plane bending and the second mode was the second out-of-plane bending. The third mode was the in-plane bending, followed by the fourth, namely torsion.
- At values from 10^6 and higher, the in-plane bending and second out-of-plane bending had crossed over, and the latter was thus the third mode now for the 0-degree and plus and minus 30-degree ply orientations. For the plus and minus 60-degree and 90-degree orientation, the in-plane bending and second out-of-plane bending did not cross over. The torsion was still the fourth mode. Depending on the coupling in the composite, the in-plane bending showed torsion effects in it.
- It was also interesting to see what happened with the second out-of-plane bending, and how it morphed. For values up to 10^4, this was the fifth mode, and only when coming close to 10^4, its frequency started rising to change to the third out-of-plane bending at a higher frequency. Explanation was as follows; the first RBM adapted the first out-of-plane bending. The second RBM changed to the second out-of-plane bending. This meant that the mode with the second out-of-plane bending before 10^4 had to change to the third out-of-plane bending.

Model with Second Laminate

- From *Figure 10*, it was clear that the root stiffness had reached a higher value before the clamped-case flutter and divergence speeds were reached. At 10^9, the speeds had just reached their clamped-case value. The eigenvalues however did not show the above behaviour. On the other hand, the frequencies were lower when compared to the first laminate.
- The ratio of the first two modes also showed another difference from the first laminate. The peak at 10^4 was still there; however, the ratios for ply angles different from 0 degree descended to a much lower value at a stiffness higher than 10^5. This was in direct response to the change in *EI*/*GJ*.
- Also, the divergence speed (*Figure 11*) was lower, but the non-dimensional divergence speed gave results very similar to the first laminate for both CAS and CUS models. The flutter speed (*Figure 10*) on the other hand showed a totally different picture. An explanation for this phenomenon was possibly found looking at the mode shapes. For the second laminate, the graph showed that the torsion was more affected by the transition of the two degrees-of-freedom from RBM to actual mode shapes. This phenomenon could trigger flutter more easily.
- As the 0-degree ply orientation had the same eigenvalues for both laminates and as the eigenfrequencies for the other ply orientations of the second laminate were lower than the first laminate as mentioned before, the peak at 0 degrees was more pronounced. This was a consistent feature too in the graphs of the ratio of the two degrees-of-freedom and the bending over torsion ratio. The physical property that showed exactly the same behaviour (a more pronounced peak) was the *EI* over *GJ* ratio. It was thus clear that the above behaviour of ratios and eigenvalues was directly dependent on the *EI* and *GJ* ratio due to the physical change in laminate.

Second Boundary Condition: Torsion and Heaving Degree of Freedom

The following results had a different boundary condition but still use the same two laminates. The two boundary condition springs now had a torsion and heaving degree of freedom. The same RBE2 set-up was used.

It immediately appeared that the behaviour of the wingbox was completely different. The results of these two laminates with this boundary condition strengthen conclusions made in previous paragraphs. They also

gave a clearer picture as to which differences could be contributed to a change in laminate and a change in boundary condition.

Model with First Laminate

- The main point of interest was that the speeds had not stabilised when reaching 10^{10} (*Figure 12* and *Figure 13*). Further analysis was necessary until at least 10^{15}. This could also be verified when comparing the speeds from the same laminate with the first boundary condition and the mode ratios (*Figure 14* and *15*). Another remarkable general difference was that the speeds tended to overshot their clamped-case value. The maximum was usually reached around 10^5. By 10^7 the speeds had come down to the clamped value.
- From *Figure 16* and *17*, the second and third mode showed clear coupling. The two first eigenvalues started out as rigid body movements, with the second mode developing in the torsion mode shape and reaching its clamped value faster than with the first boundary condition. Remark that where in the previous case the torsion frequency was unaffected by the change in second out-of-plane bending; here these two showed clear interaction. The visualisation of the mode shapes explained this behaviour: the final torsion mode (so the third) started out as a weak out-of-plane bending movement. When the second and the third mode crossed over, the third started evolving to a torsion mode and the second mode evolved to a second out-of-plane bending. Another proof of this was that in contrast with the first boundary condition, the second mode did not go down all the way to zero at 10^0. Also the third mode was normally not affected by a change in root stiffness, which it was with this boundary condition.
- Interestingly enough, in the same *Figures 16* and *17*, the third out-of-plane bending mode shape was relatively unaffected by this coupling. It was logical from this perspective, that now there was a torsion spring instead of a bending spring, but it contradicted all the interactions summed up in the previous point.

Model with second laminate

- When the second laminate was discussed with the first boundary condition, it appeared that some changes in physical properties could be directly related to the modal response, flutter, and divergence speed. It was clear that the same trends were visible here. Especially the flutter speed (*Figure 18*) showed similar behaviour as when comparing the two laminates with the bending and heaving spring. It was logical that those differences already summed up in previous paragraphs could be contributed to the change in physical properties of the laminate.
- When plotting the eigenvalues versus root stiffness for different fibre orientations, a sharper peak appeared just like the *EI*/*GJ* ratio changes between the two laminates. This showed that the eigenvalues were indeed directly influenced by the physical property change, as expected.
- The development of the eigenvalues did not show a significant difference from the previous laminate however, indicating that the activity summed up in the previous section was entirely due to the different boundary condition.

CONCLUSIONS

The research showed that the root stiffness had a significant influence on the modal response of a wing. It also showed that this behaviour influenced the aeroelastic properties of the lifting surface. It was possible to explain the change in modal response; however, it proved more research was needed to clarify the influence of the root stiffness on aeroelastic properties as flutter and divergence speed. More information on the mechanism was needed.

The eigenvalues for both boundary condition showed a clear interaction with the *EI*/*GJ* ratio. Some changes in flutter and divergence speed were recognised as being a direct effect of the physical changes in laminate or boundary condition. Nonetheless, additional research was still needed to explain certain peaks and dips that had no significant origin. Georghiades and Banerjee (*Ref. 6*) gave a possible explanation as what could be a plausible reason: modal interchange. It is possible that the modal interchange influences the aerodynamics over the wing and induces flutter and divergence. A more detailed analyses is still needed.

Due to the coarse ply degree step (30 degrees) it was difficult to make conclusions as it was well known that composites can have totally different properties by just changing the ply angel 5 degrees. It also proved to be difficult to relate physical property changes to the actual change in model behaviour.

The first two variables – fibre orientation and ply stacking sequence – were modelled with finite elements in the past. The computational results were validated with experimental research. However, the results and conclusions made with respect to the root flexibility were not experimentally supported. An experimental set-up could also help to understand the exact influence of the root flexibility. Alternative ways

of modelling the root flexibility in the finite element code could then also be investigated. More specifically, Llamas Sandin (*Ref. 10*) used a different approach in which multiple springs were attached at discrete wing root points. This could be included in this research to assess differences in both methods. It could also validate the current modelling approach.

It is also important to note that during the course of this research no values were found for the root stiffness of real aircraft structures. Thus it was not exactly clear in which region real aircraft structures operate, although it was obvious that those will tend to be on the stiffer side, where a change in stiffness has little effect on flutter and divergence speed.

REFERENCES

1. Battoo, R.S., "MSC/NASTRAN Dynamic Analysis of a Composite Wingbox Structure," Presented at the 1998 MSC users conference in Solihul, Birmingham, England, UK, June 1998

2. Cesnik, C.E., Hodges, D.H., and Patil, M.J., "Aeroelastic Analysis of Composite Wings," *Proceedings of the 37th AIAA, ASME, ASCE, and AHS, Structures, Structural Dynamics, and Materials Conference and Exhibit*, Salt Lake City, UT, Apr. 15-17, 1996, Technical Papers Pt. 2, p. 1113-1123

3. Chandra, R., Stemple, A.D., and Chopra, I., "Thin-Walled Composite Beams under Bending, Torsional, and Extensional Loads," *Journal of Aircraft*, vol. 27, July 1990, p. 619-626

4. De Baets, P.W.G. , Aeroelastic Analysis of a Composite Wingbox with Varying Root Flexibility and Skin Lay-up Using Finite Element Modelling," Cranfield University, England, UK, MSc Thesis 1999

5. Doggett, R.V.Jr., and Soistmann, D.L., "Low-Speed Flutter Characteristics of Some Simple Low-Aspect-Ratio Delta-Wing Models," *Proceedings of the 30th AIAA, ASME, ASCE, AHS, and ASC, Structures, Structural Dynamics and Materials Conference*, Mobile, AL, Apr. 3-5, 1989, Technical Papers. Pt. 3, p. 1442-1450

6. Georghiades, G.A., and Banerjee, J.R., "Role of Modal Interchange on the Flutter of Laminated Composite Wings," *Journal of Aircraft*, vol. 35, no. 1, Jan.-Feb. 1998, p. 157-161

7. Georghiades, G.A., and Banerjee, J.R., "Flutter Prediction for Composite Wings using Parametric Studies," *Proceedings of the 37th AIAA, ASME, ASCE, and AHS, Structures, Structural Dynamics, and Materials Conference and Exhibit*, Salt Lake City, UT, Apr. 15-17, 1996, Technical Papers. Pt. 1, p. 300-310

8. Johnson, E.H. and, Neill, D.J., "Automated Structural Optimisation System (ASTROS), Volume III – Applications Manual," Wright Laboratory AFWAL-TR-88-3028, December 1988

9. Johnson, E.H. and, Venkayya, V.B., "Automated Structural Optimisation System (ASTROS), Volume I – Theoretical Manual," Wright Laboratory AFWAL-TR-88-3028, December 1988

10. Llamas Sandin, R.C., "Flutter Analysis of A Delta Wing for Variations in Attachment and Actuator Stiffness," Cranfield University, England, UK, MSc Thesis 1997

11. Neill, D.J., Johnson, E.H., and Canfield, R.A., "ASTROS – A Multidisciplinary Automated Design Tool," *Journal of Aircraft*, vol. 27, No. 12, 1990, pp. 1021-1027

12. Shirk, M.H., Hertz, T.J., and Weisshaar, T.A., "Aeroelastic Tailoring – Theory, Practice, and Promise," *Journal of Aircraft*, vol. 23, Jan. 1986, p. 6-18.

13. Striz, A.G., and Venkayya, V.B., "Influence of Structural and Aerodynamic Modelling on Flutter Analysis," *Journal of Aircraft*, vol. 31, No. 5, 1994, p. 1205-1211

14. Weisshaar, T.A., and Ryan, R.J., "Control of aeroelastic instabilities through stiffness cross-coupling," *Proceedings of the 25th AIAA, ASME, ASCE, and AHS, Structures, Structural Dynamics and Materials Conference*, Palm Springs, CA, May 14-16, 1984, Technical Papers. Part 2, p. 226-235

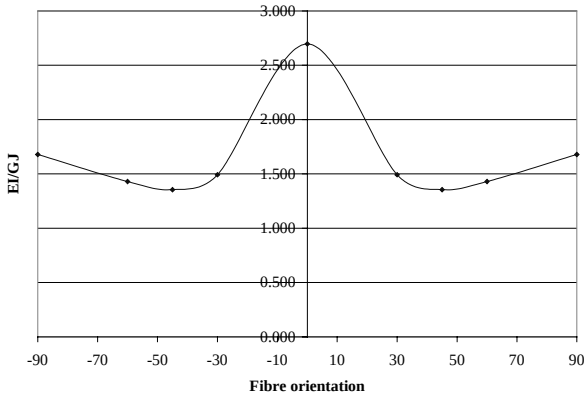

Figure 3 EI/GJ versus fibre orientation (Laminate 1)

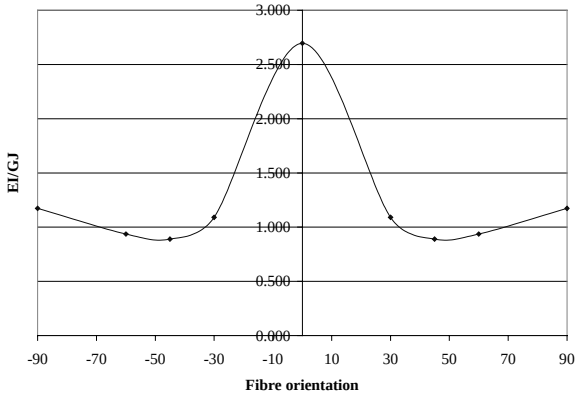

Figure 4 EI/GJ versus fibre orientation (Laminate 2)

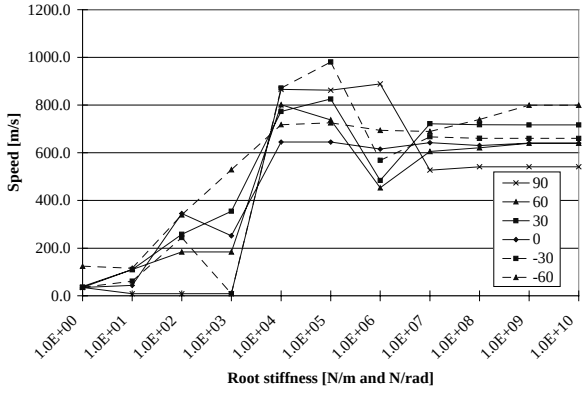

Figure 5 Flutter speed versus fibre orientation and root stiffness (Boundary Condition 1, Laminate 1, CAS)

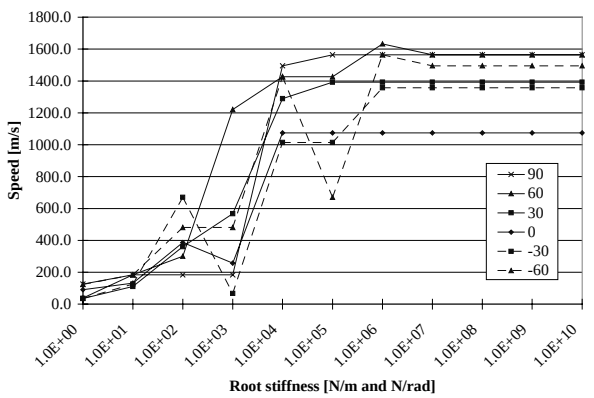

Figure 6 Divergence speed versus fibre orientation and root stiffness (Boundary Condition 1, Laminate 1, CAS)

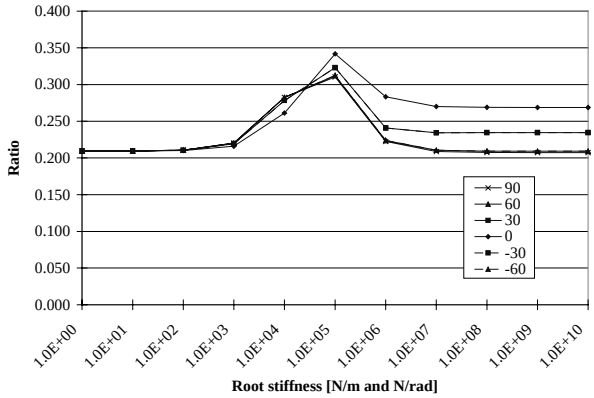

Figure 7 Out-of-plane bending over second out-of-plane bending versus fibre orientation and root stiffness (Boundary Condition 1, Laminate 1, CAS)

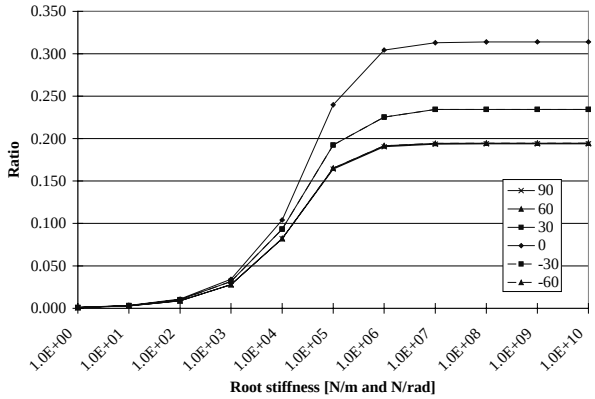

Figure 8 Out-of-plane bending mode over torsion mode speed versus fibre orientation and root stiffness (Boundary Condition 1, Laminate 1, CAS)

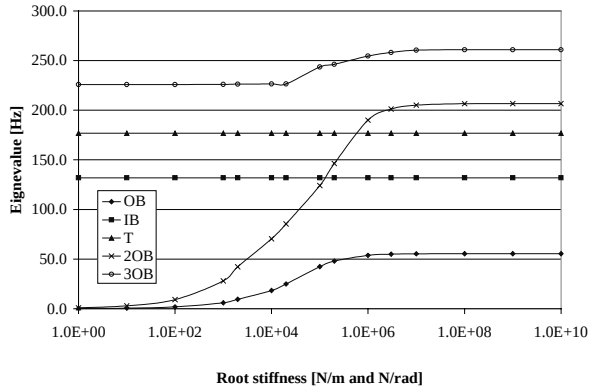

Figure 9 Eigenvalues versus root stiffness (Boundary Condition 1, Laminate 1, 0-degree fibre orientation, CAS)

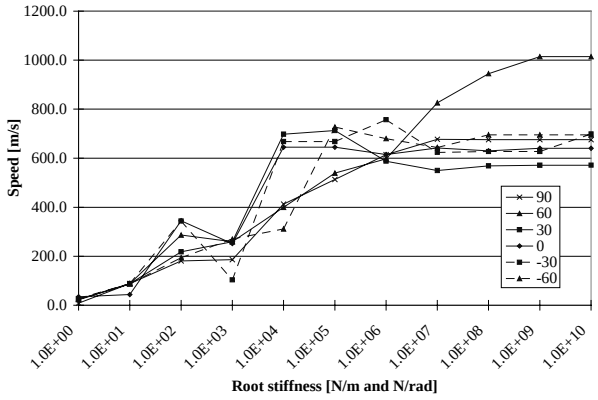

Figure 10 Flutter speed versus fibre orientation and root stiffness (Boundary Condition 1, Laminate 2, CAS)

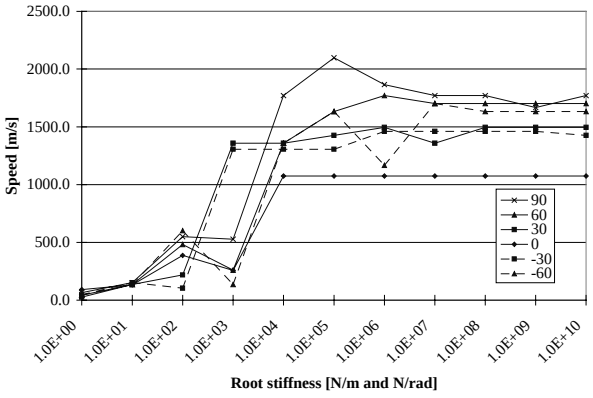

Figure 11 Divergence speed versus fibre orientation and root stiffness (Boundary Condition 1, Laminate 2, CAS)

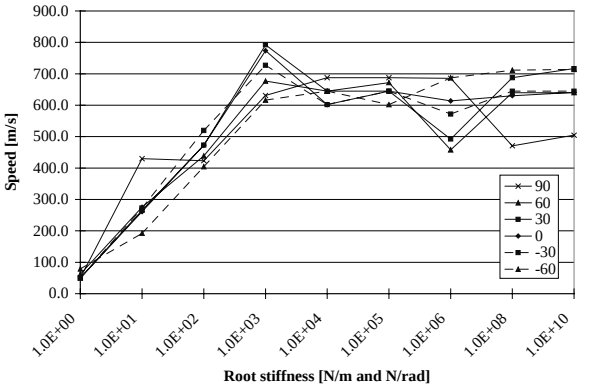

Figure 12 Flutter speed versus fibre orientation and root stiffness (Boundary Condition 2, Laminate 1, CAS)

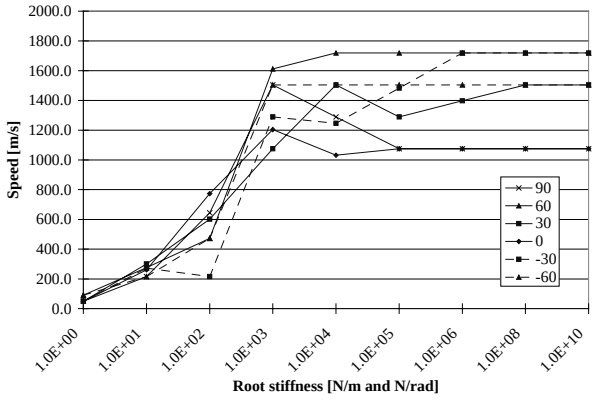

Figure 13 Divergence speed versus fibre orientation and root stiffness (Boundary Condition 2, Laminate 1, CAS)

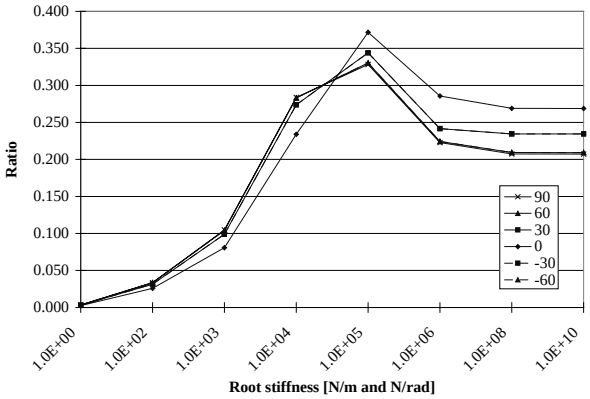

Figure 14 Out-of-plane bending over second out-of-plane bending versus fibre orientation and root stiffness (Boundary Condition 2, Laminate 1, CAS)

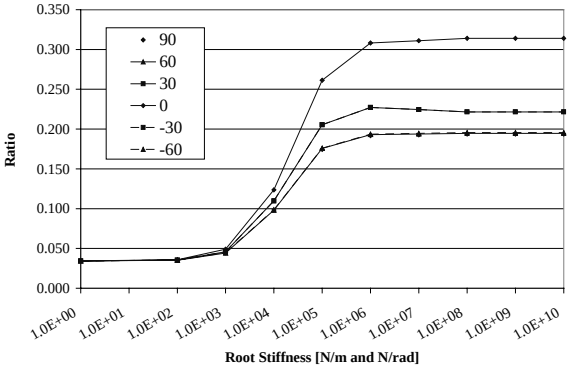

Figure 15 Out-of-plane bending mode over torsion mode speed versus fibre orientation and root stiffness (Boundary Condition 2, Laminate 1, CAS)

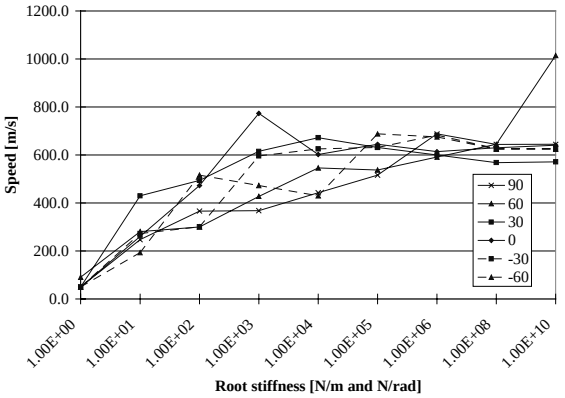

Figure 18 Flutter speed versus fibre orientation and root stiffness (Boundary Condition 2, Laminate 2, CAS)

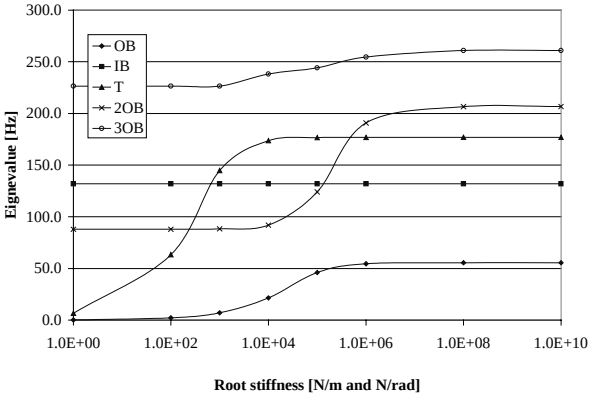

Figure 16 Eigenvalues versus root stiffness (Boundary Condition 2, Laminate 1, 0-degree fibre orientation, CAS)

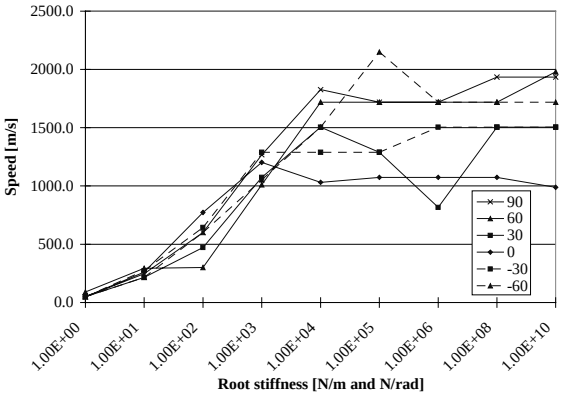

Figure 19 Divergence speed versus fibre orientation and root stiffness (Boundary Condition 2, Laminate 2, CAS)

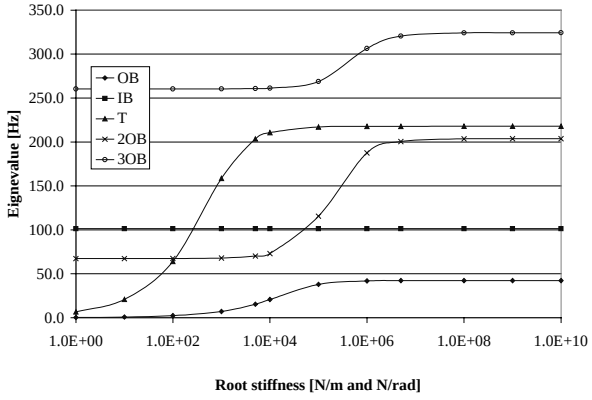

Figure 17 Eigenvalues versus root stiffness (Boundary Condition 2, Laminate 1, 90-degree fibre orientation, CAS)